Structure
Article

Structure and Membrane Interaction of Myristoylated ARF1

Yizhou Liu,[1] Richard A. Kahn,[2] and James H. Prestegard[1,*]
[1]Complex Carbohydrate Research Center, University of Georgia, 315 Riverbend Road, Athens, GA 30602-4712, USA
[2]Department of Biochemistry, Emory University School of Medicine, 1510 Clifton Road, Atlanta, GA 30322-3050, USA
*Correspondence: jpresteg@ccrc.uga.edu
DOI 10.1016/j.str.2008.10.020

SUMMARY

ADP-ribosylation factors (ARFs) are small (21 kDa), monomeric GTPases that are important regulators of membrane traffic. When membrane bound, they recruit soluble adaptors to membranes and trigger the assembly of coating complexes involved in cargo selection and vesicular budding. N-myristoylation is a conserved feature of all ARF proteins that is required for its biological functions, although the mechanism(s) by which the myristate acts in ARF functions is not fully understood. Here we present the structure of a myristoylated ARF1 protein, determined by solution NMR methods, and an assessment of the influence of myristoylation on association of ARF1·GDP and ARF1·GTP with lipid bilayers. A model in which myristoylation contributes to both the regulation of guanine nucleotide exchange and stable membrane association is supported.

INTRODUCTION

ADP-ribosylation factors (ARFs) are ~20 kDa GTPases that have been very highly conserved throughout eukaryotic evolution, are ubiquitously expressed in eukaryotic organisms, and play essential roles in the regulation of membrane traffic (Gillingham and Munro, 2007; Nie et al., 2003; Donaldson et al., 2005). ARFs interact with a number of proteins at membrane surfaces, including guanine nucleotide exchange factors (GEFs) that facilitate GDP for GTP exchange (Peyroche et al., 1996; Chardin et al., 1996), GTPase activating proteins (GAPs) that impart GTPase activity (Cukierman et al., 1995; Inoue and Randazzo, 2007), enzymes involved in lipid metabolism (Brown et al., 1993; Godi et al., 1999, 2004), and the protein adaptors that aid in the recruitment of specific cargos (Serafini et al., 1991; Bonifacino, 2004; Styers and Faundez, 2004; Hill et al., 2003). A central aspect of ARF-dependent cell regulation is their cycling between the predominantly cytosolic GDP-bound and the membrane-associated GTP-bound forms. Alterations in the exposure of both an N-terminal myristoyl group and an N-terminal amphipathic helix upon nucleotide exchange have been postulated to play roles in membrane association and dissociation. However, confirmation of these changes through structural investigations has been difficult because recombinant protein preparations available in the required quantities lack the N-terminal myristoyl group and, in some cases, the critical N-terminal amino acids as well. Because the presence of activated, membrane-associated ARF is viewed as the critical initiator of vesicle biogenesis, the molecular details of the processes of membrane association and activation are essential to the generation of models of membrane traffic.

Early models of ARF-membrane interaction postulated that the exchange of GTP for GDP caused exposure of the myristoyl group and that myristoyl-lipid interaction subsequently recruited ARF to the membrane (Helms et al., 1993; Tanigawa et al., 1993). This is similar to the calcium-switch mechanism postulated for recoverin (Zozulya and Stryer, 1992). However, other data cast doubts on this simple model. First, nonmyristoylated ARF was shown to be capable of stable membrane interaction through the N terminus, raising questions regarding the function of the highly conserved myristoyl group (Franco et al., 1993). Second, a high concentration of phospholipids is normally required for guanine nucleotide exchange, as catalyzed by ARF GEFs (Franco et al., 1996). This suggests that the membrane surface may actually provide a platform essential for the exchange reaction. This suggestion is consistent with the observations that the rate of dissociation of the tightly bound GDP is increased in the presence of lipids, detergents, or membranes (Weiss et al., 1989). Together, these observations open the possibility that myristoyl insertion into the membrane is not a simple consequence of guanine nucleotide exchange but that it may play earlier roles in the overall processes of membrane association, ARF activation, and recruitment of GEFs, GAPs, and effectors.

Crystal structures exist for GDP-bound forms of full-length human ARFs lacking myristate and GTP-loaded forms of ARFs lacking the N-terminal 17 residues (ARF1Δ17) as well as myristate (Amor et al., 1994; Goldberg, 1998). ARF1Δ17 has improved solubility and is able to undergo efficient guanine nucleotide exchange in the absence of a GEF without the requirements for phospholipids or detergents (Kahn et al., 1992). These features facilitated the later structural study which, together with the earlier one, provided significant insight into the mechanisms of guanine nucleotide exchange and hydrolysis. However, truncation of the N terminus introduces ambiguity because structures thus obtained may carry artifacts resulting from the N-terminal deletion (Seidel et al., 2004). Previously, we have shown that substantial structural discrepancies exist between ARF1·GDP and ARF1Δ17·GDP, and thus it is necessary to deconvolute such differences from other sources of structural changes, such as those from nucleotide exchange (Seidel et al., 2004). Moreover, the lack of the N-terminal residues and

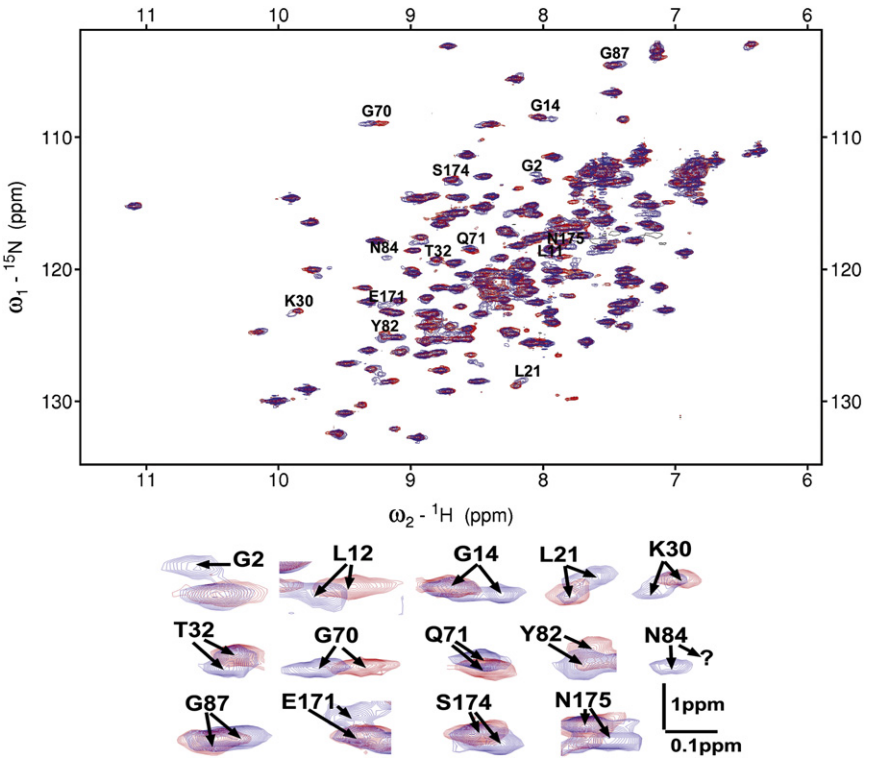

Figure 1. ^{15}N-^{1}H HSQC Spectra of myr(+)- and myr(−)-yARF1·GDP

myr(+)- and myr(−)-yARF1·GDP are shown in blue and red, respectively. Blown-up views of chemical shift perturbed residues are displayed on the bottom.

the myristoyl group precludes investigation of the role of myristoylation and the N-terminal amphiphilic region in events such as membrane association/dissociation, nucleotide exchange, and GTP hydrolysis. Clearly, extending studies to a myristoylated form of ARF in a relatively native lipid-containing environment promises to yield novel and significant understanding of the biological activities of ARF.

Changes in solubility and crystallization properties upon myristoylation have posed difficulties for structural determination by both X-ray crystallography and NMR. Multidimensional heteronuclear NMR, and more recent experimental developments such as transverse relaxation optimized spectroscopy (TROSY) (Pervushin et al., 1997), residual dipolar coupling (RDC) measurement (Tolman et al., 1995; Tjandra and Bax, 1997), and methyl protonation with background perdeuteration of samples (Rosen et al., 1996), have greatly improved the prospects for structural and dynamic studies on large proteins and membrane proteins by NMR. NMR has, in fact, been used to study myristoylated proteins, but only in a few cases (Tanaka et al., 1995; Tang et al., 2004). Prerequisite to such studies is actual production of a myristoylated protein. In this study, the yeast *Saccharomyces cerevisiae* ARF1 (yARF1) was adopted due to its high myristoylation efficiency when coexpressed in bacteria with an N-myristoyltransferase (Randazzo and Kahn, 1995). Human and yeast ARF1 share >74% identity, and the fact that human protein can complement the deletion of yARF1 is indicative of close functional and structural conservation despite the evolutionary distance between these organisms (Kahn et al., 1991; Logsdon and Kahn, 2004). Here these favorable properties have been used to determine a solution structure of the myristoylated form of yARF1·GDP along with data on the interaction of both the GDP-bound and GTP-bound forms with membrane mimetics. The structure clearly places the myristoyl chain in a hydrophobic groove between a C-terminal helix and a loop connecting β strands 3 and 4. The positioning suggests a clash with this loop would occur as it exists in the GTP-bound form, a fact that may require membrane association to accommodate an expelled myristoyl chain before GDP exchange can occur. The data on interaction with membrane mimetics show that myristoylation enhances membrane interactions of both GDP and GTP forms of yARF1. The interactions of the GDP form are weaker, but they also display an interesting preference for interaction with more extended membrane structures that may be of functional significance.

RESULTS AND DISCUSSION

Structure Determination

Yeast ARF1 was expressed in bacteria either alone (myr[−]) or coexpressed with the yeast N-myristoyltransferase NMT1 to generate the acylated (myr[+]) protein. The extensive similarity between the HSQC spectra of myr(+) and myr(−)-yARF1·GDP indicates that myristoylation does not extensively alter the global fold of yARF1 (Figure 1). However, specific changes in positions or intensities of resonances from sites throughout the protein suggest that effects of myristoylation on structure do occur and these may have biological consequences. Some of the affected residues are near the N terminus where anticipated, for example, G2 is invisible in myr(−)-yARF1 but shows up in myr(+)-yARF1 due to the quenched amine proton exchange rate upon myristoyl conjugation. Other perturbed N-terminal residues include L12 and G14. Perturbed residues more C terminal in the sequence include those traditionally associated with functionally important parts of the protein, including switch II (G70, Q71, and Y82), the nucleotide binding site (K30 and T32), and the C-terminal helix (E171, S174, and N175).

Numerous perturbed resonances also display some level of heterogeneity. These include G14, L21, K30, T32, E171, S174, and N175, where two sets of resonances are observed upon acylation. One of the members of the pairs is usually minimally perturbed from that of myr(−) and the other is shifted substantially (Figure 1). This could result from partial N-myristoylation of the yARF1 in bacteria. Closer examination by electrospray

ionization mass spectrometry and fatty acid analysis revealed that greater than 90% of the purified protein is acylated, but only ~50% is myristoylated while the remaining ~40%–50% is lauroylated. The presence of covalently attached laurate on yARF1 is presumably caused by the broader specificities for fatty acids (Kishore et al., 1993) of yeast or human NMT1 when expressed in bacteria and differences in the levels of acyl-coA substrates among organisms. Incorporation of acyl chains other than myristate into ARF proteins coexpressed in bacteria with NMT has been reported previously (Randazzo and Kahn, 1995), although in that report the diversity of acyl chain lengths was much greater. Because lauroyl-ARF1 differs from the physiologically relevant myristoyl-ARF1 by only two carbons, and the acyl chain is relatively unstructured (see below), we believe it is unlikely the heterogeneity in the acyl group compromises conclusions drawn. Nevertheless, in an effort to resolve the effects of the different acyl groups, an isotope labeling strategy was employed in which myristate and laurate were isotope labeled differently and X-filtered NMR experiments were applied to help suppress the N-lauroyl-yARF1 signals (see Experimental Procedures).

Several types of structural data were acquired (Table 1) including distance restraints between (1) amide protons, (2) amide and a number of side-chain methylene/methyl protons, (3) sets of methyl protons, (4) amide and myristoyl protons, and (5) methyl and myristoyl protons. RDCs were collected from a compressed charged gel and a stretched neutral gel which yielded two uncorrelated alignment conditions and therefore two sets of complementary RDC data. The presence of bound GDP is confirmed from six assigned nuclear Overhauser effects (NOEs) between the protein amides and the labile HN_1 proton of the guanine base (other GDP protons are invisible due to perdeuteration or fast solvent exchange). Given the consistency of these NOEs with what is expected from the crystal structures of ARF·GDP, conserved hydrogen bonds between ARF and GDP observed in the crystal structures were utilized to help restrain the nucleotide during structure calculations. The structure was solved applying these restraints in a simulated annealing protocol run under the program CNS (Brünger et al., 1998).

Table 1. Statistics of Structure Calculations Based on 15 Accepted Structures

Total NOEs observed	1398
Total nonredundant NOEs	830
Intraresidue (i = j)	182
Sequential (|i − j| = 1)	272
Medium-range (1 < |i − j| < 5)	146
Long-range (|i − j| > 4)	173
Ambiguous	57
ARF-myristoyl NOEs	14
ARF-GDP NOEs	6
Dihedral angle restraints	
Φ	101
Ψ	100
Residual dipolar couplings[a]	
HN (alignment 1 + alignment 2)	108 + 99
NC′ (alignment 1)	58
HNC′ (alignment 1)	57
Hydrogen-bond restraints	180
Rmsd of distance violations (maximum) (Å)	0.0136 ± 0.0005 (0.129 ± 0.017)
Rmsd of dihedral angle violations (maximum) (°)	0.371 ± 0.026 (2.05 ± 0.58)
Rmsd of RDC violations (Hz)/maximum of RDC (Hz)	
HN (alignment 1)	1.49 ± 0.06/22.45 ± 0.13
HN (alignment 2)	1.82 ± 0.03/20.31 ± 0.14
NC′ (alignment 1)	0.26 ± 0.02/2.72 ± 0.02
HNC′ (alignment 1)	0.77 ± 0.02/7.12 ± 0.04
Rmsd of covalent geometry	
Bond lengths (Å)	0.0017 ± 0.00003
Bond angles (°)	0.3537 ± 0.0035
Impropers (°)	0.2872 ± 0.0104
Ramachandran plot statistics (%)	Residues (18–71, 77–178)
Most favored	91.4
Additionally allowed	5.7
Generously allowed	0
Disallowed	2.9
Rmsd for NMR ensemble (Å)	Residues (18–71, 77–178)
Backbone	0.762
Heavy atoms	1.391

[a] HN RDCs were collected for two highly uncorrelated alignments. Alignment 1 is by negatively charged compressed gel and alignment 2 is by neutral stretched gel. See Experimental Procedures for details.

Structure of myr(+)-yARF1·GDP

Myristoylated yARF1·GDP in solution adopts an overall fold that is very similar to the nonmyristoylated ARF proteins whose crystal structures have previously been reported (Amor et al., 1994, 2001). A superposition of 15 of the lowest-energy structures is depicted in Figure 2A (a stereo view of the superimposed structures is given in Supplemental Data available online). The N terminus (G2–N15) and part of switch II (D72–S76) are not well defined because a majority of residues in these regions lack detectable NMR signals, presumably due to the presence of multiple conformational states interconverting on the μs-ms timescale.

Myristoyl chain representations (Figure 2, purple) are also not particularly closely clustered but clearly sequestered in an extended hydrophobic groove lined by multiple nonsequential residues, including L12*, I20*, L37, Y58, I61, I89*, L170*, L173*, and L177 (NOEs to the myristoyl group were detected for residues marked with an asterisk). The distribution of the myristoyl group structures may reflect a certain level of mobility or the absence of sufficient NOE constraints along the central region of the myristoyl chain. The hydrophobic pocket buries roughly half the myristoyl chain while the other half is kept from the solvent by an overlay of the N terminus. In crystal structures of full-length myr(−)-ARF proteins and NMR structures of the isolated myr(+)-N terminus, the N-terminal residues generally form an amphipathic helix, the length of which varies among different ARF proteins (Amor et al., 1994, 2001; Losonczi and Prestegard, 1998; Gizachew and Oswald, 2006). A

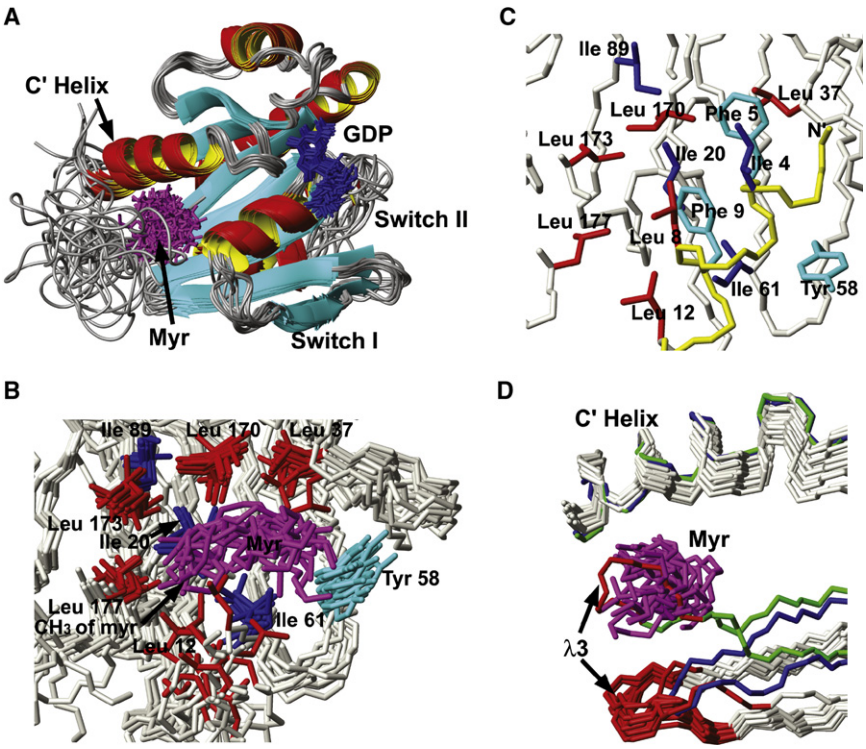

Figure 2. Structure of Myristoylated yARF1 and Comparisons to Related Structures

(A) Overlap of 15 accepted myr(+)-yARF1·GDP structures out of 100 trials. GDP is shown in blue and myristoyl is in purple.

(B) The myristoyl binding pocket with leucines shown in red, isoleucines in blue, tyrosines in cyan, and myristoyl in purple.

(C) The myristoyl binding pocket lies under the N-terminal amphiphilic helix in the myr(−)-hARF·GDP structure (Protein Data Bank ID code 1hur).

(D) The interstrand loop λ3 clashes with the myristoyl chain in the GTP-bound conformation but not in the GDP-bound conformation. The backbone of myr(+)-yARF1·GDP is shown in ivory, myr(−)-hARF1·GDP in blue, and hARF1Δ17·GTP in green. λ3 of all molecules is shown in red, and myristoyl is shown in purple.

high-resolution picture of the N terminus is unavailable in our structure due to the broadened or missing resonances of this region, but it is tempting to speculate that the hydrophobic face of the amphiphilic helix faces the myristoyl chain, with the hydrophilic face solvent exposed. The severe line broadening and absence of resonances is consistent with interchange of multiple N-terminal conformations of comparable free energy. A similar statement can be made for missing residues in switch II. The high structural plasticity of these regions may be related to the need for dramatic conformational change during guanine nucleotide exchange and myristoyl chain exposure. Interestingly, the myristoyl group is not proximal to switch II or the GDP binding site, although these regions display perturbed chemical shifts upon myristoylation (Figure 1). Instead, the acyl chain may have an allosteric effect on nucleotide exchange properties, consistent with the myristate playing a role as a clamp to slow GDP dissociation and prevent spontaneous nucleotide exchange in aqueous solution, as seen earlier in nucleotide binding and exchange assays (Randazzo et al., 1995).

The myristoyl binding pocket can be recognized in the crystal structure of myr(−)-yARF2·GDP (Amor et al., 2001), but it is partly shielded from water by the hydrophobic face of the N-terminal helix (Figure 2C). In the GTP-bound conformation as shown in the crystal structure of hARF1Δ17 (Goldberg, 1998), the displacement of the β2-β3 strands shifts the interswitch loop λ3 (E57–I61) into the myristoyl binding pocket; this is predicted to lead to steric clashes preventing myristoyl sequestration (Figure 2D). Structural comparison of myr(−)-ARF·GDP and ARFΔ17·GTP had previously suggested that intrusion of λ3 is responsible for myristoyl release during guanine nucleotide exchange by sterically expelling the N-terminal helix (Goldberg, 1998; Renault et al., 2003). Here it is clear that the positional change of λ3 leads directly to interference with myristoyl binding, rather than through an indirect effect on the N-terminal helix.

myr(+)-yARF1·GDP Weakly Interacts with Lipids

To assess membrane interactions, a number of experiments designed to examine changes in motional correlation times on exposure to model membranes were employed. The effective rotational correlation time (τ_c), measured from NMR relaxation experiments or reflected in NMR spectral line widths, is closely related to the tumbling rate of a molecule in solution. Therefore, assuming other factors, such as temperature and viscosity, remain constant, it reports on the apparent molecular size. Association of ARF with membrane-like fragments should clearly lead to an increased effective size and an increase in correlation times. To extract correlation times (τ_c), a previously published NMR technique (Liu and Prestegard, 2008) was applied to yARF1 in the presence and absence of lipid bicelles. Initially, a small bicelle system was utilized as a membrane mimic; it consists of dimyristoyl-phosphatidylcholine (DMPC) and dihexanoyl-phosphatidylcholine (DHPC) at a 1:4 molar ratio (q = [DMPC]:[DHPC] = 0.25). This ratio yields bicelle disks with a radius of ~24 Å and thickness of ~40 Å (Glover et al., 2001; Luchette et al., 2001). Complete association of ARF with this fragment should roughly double the effective correlation time, but still provide favorable high-resolution NMR spectra.

The ^{15}N spin relaxation experiments show relatively little variation in τ_c determinations with residue position, particularly in the C-terminal half of the protein (Figures 3A and 3B). These invariant regions report most directly on overall correlation time. Both myr(+)- and myr(−)-yARF1·GDP displayed modestly elevated τ_cs for residues in these regions (40% and 34%, respectively) in the presence of 10% (w/v) lipids (Figures 3A and 3B). This can be interpreted as weak lipid interaction, but it may also be an effect of increased solution viscosity. Estimations based on a modified Stokes-Einstein-Debye equation predict a 20% increase in rotational correlation time due to viscosity changes upon the addition of small bicelles (Ross and Minton, 1977;

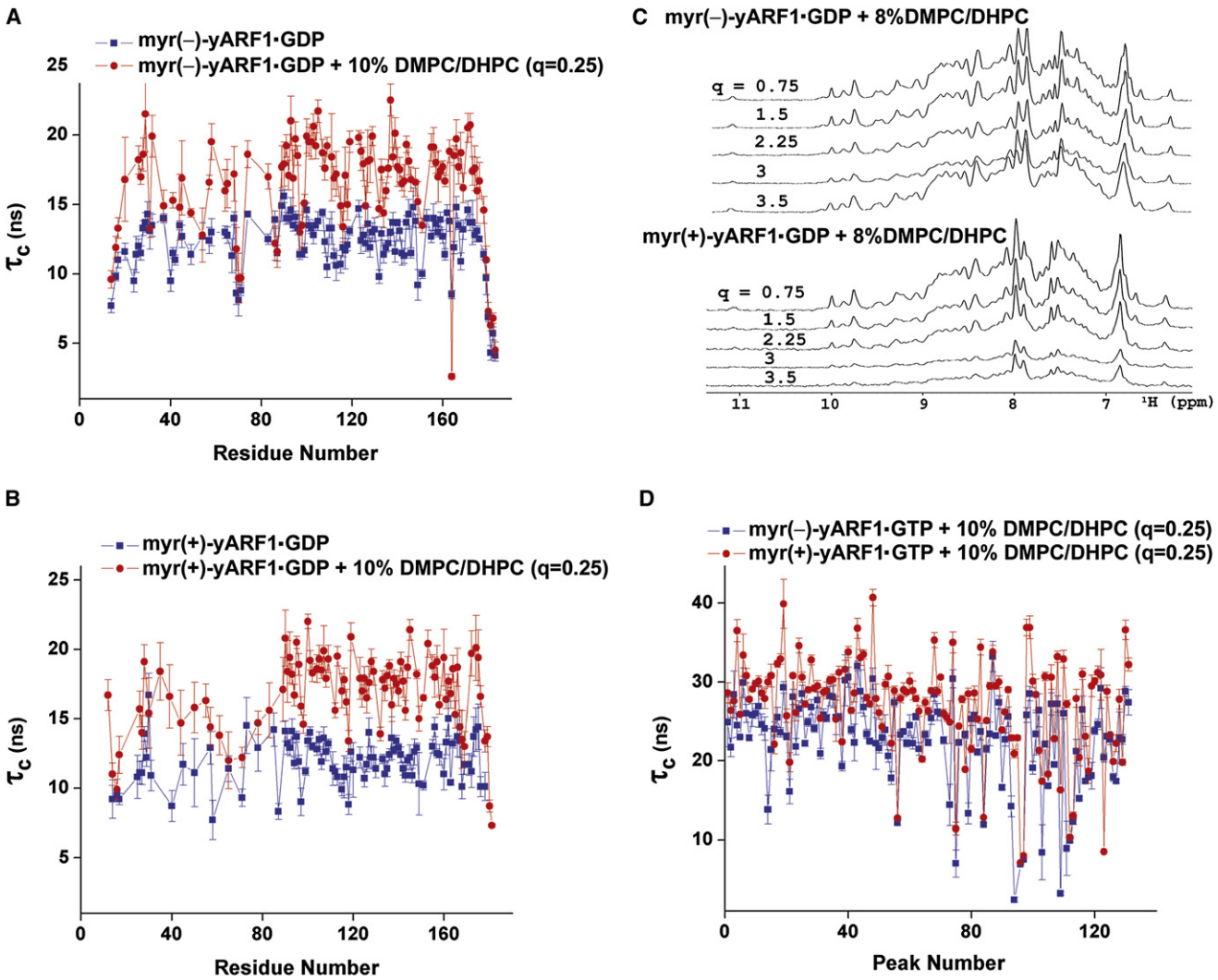

Figure 3. Interaction of yARF1 with Lipid Bicelles

(A and B) The residue-specific effective rotational correlation times of myr(−)- and myr(+)-yARF1·GDP in the absence or presence of 10% DMPC/DHPC small bicelles.

(C) One-dimensional ^{15}N-^{1}H HSQC scans of myr(−)- and myr(+)-yARF1·GDP mixed with DMPC/DHPC bicelles of varying sizes.

(D) Effective rotational correlation times of myr(−)- and myr(+)-yARF1·GTP in the presence of 10% DMPC/DHPC small bicelles.

Lavalette et al., 2006). Given the approximations in this equation, the observed change in correlation times could largely result from the change in viscosity. It is notable that the changes are approximately the same for both myr and non-myr forms. The lack of an observable enhanced interaction for the GDP-loaded, myristoylated form could be a consequence of the stability of the myristoyl chain in the well-shielded binding pocket relative to its stability in the small bicelle structure. Small levels of interaction may also be difficult to detect given the modest increase in effective molecular size on interaction with small bicelles.

It is possible to further distinguish viscosity effects from effective size effects, as well as improve sensitivity to association, using an experiment in which the lipid concentration is fixed at 8% (in order to minimize the viscosity changes) while varying the bicelle size by adjusting the q value. The q values of 0.75, 1.5, 2.25, 3.0, and 3.5 correspond to bicelle disk radii of 57.5, 105.6, 153.1, 200.5, and 232 Å (Vold and Prosser, 1996). The bicelle thickness is independent of q and stays at ~40 Å in this simplified bicelle model (Vold and Prosser, 1996). This progressive increase in bicelle size with q value increases sensitivity to weak protein interactions as it produces increasingly larger changes in correlation time upon bicelle interaction.

For the experiments with larger bicelles, a 1D ^{15}N-^{1}H HSQC experiment was used to monitor τ_c changes as reflected in signal intensity changes. Due to the exponential decay of transverse magnetization during coherence transfer between nuclei (INEPT and reverse-INEPT steps) in HSQC experiments, and the direct dependence of this decay on τ_c for most resonances, peak intensity in 1D HSQC experiments is a sensitive reporter of changes in τ_c. Whereas myr(−)-yARF1·GDP has minimal dependence on bicelle size within the examined range (Figure 3C, upper panel), myr(+)-yARF1·GDP showed a marked decrease in

intensity at q = 3.0 and above (Figure 3C, lower panel). Because the viscosity is identical for myr(+) and myr(−) samples at the same q value, the differential dependence of intensity on the q ratio can be directly correlated to the differential lipid interaction tendencies of the two forms of the GDP-loaded protein. Note that this is not necessarily inconsistent with the τ_c data reported in Figure 3B, which reports only data collected at relatively low q value (0.25). One interpretation of the data in Figures 3A–3C is that myr(+)-yARF1·GDP does interact more strongly with bicelles than does myr(−)-yARF1·GDP, although this interaction is still relatively weak and undergoes fast exchange. As a result, this difference between myr(+) and myr(−) proteins is best seen at higher q values, where lipid association has more exaggerating effects on the rotational correlation time. However, an alternate interpretation of these data is that there may be preferential interaction of myr(+)-yARF1·GDP with bicelles of higher q values because they display a more planar membrane character, or a surface region that is simply more compatible with myristoyl chain insertion (DMPC acyl chains are well matched to the myr[+] chain length). In the ideal bicelle model, the short-chained DHPC molecules form the rim of the disc, whereas the long-chained DMPC molecules are segregated in the center. However, near the interface of DHPC and DMPC, neither could be ideally packed due to the mismatch in chain length. Thus, at low q values, a significant percentage of DMPC could be in this loosely packed region, which does not represent an ideal binding surface for ARF. As the q value increases, more planar regions with compatible chain lengths would form in the center of the disc, and this might lead to a more stable interaction with ARF. Recognition of a planar surface is a particularly attractive possibility because it could reflect an important extension of the current model that some ARF GAPs are activated by increases in membrane curvature (Bigay et al., 2003, 2005). Thus, the cycle of ARF activation/deactivation would be coupled at both ends if myr(+)ARF·GDP is first attracted to planar membranes, where it interacts with an ARF GEF to generate activated myr(+)ARF·GTP, and recruit adaptors required for specific carrier biogenesis and membrane deformation, leading to ARF GAP activation, GTP hydrolysis, and release of the resulting myr(+)ARF·GDP to the cytosol.

Once associated with a membrane surface, it is interesting to consider what changes in protein structure would be required for, or result from, insertion of myristate into the bilayer. A direct insertion of the myristoyl chain would necessarily involve displacement of the N terminus, as it keeps the myristoyl chain hidden from the solvent in the absence of lipids. Previous studies have shown that myr(+)-ARF·GDP requires both GEF and high concentrations of phospholipids for efficient guanine nucleotide exchange at physiological Mg^{2+} concentrations (Franco et al., 1996), whereas ARFΔ17-GDP only requires GEF (Goldberg, 1998). This suggests that displacement of the N terminus, whether by actual deletion from the protein sequence or by a lipid environment favoring exposure of the myristoyl chain, can facilitate nucleotide exchange. Based on the crystal structure of hARF1Δ17 complexed with a Sec7 domain (Goldberg, 1998), a GEF promotes guanine nucleotide exchange by inducing a nucleotide-free form of ARF that structurally resembles the GTP-bound form, a conformation also promoted by N-terminal deletion (Seidel et al., 2004). According to the structure presented here, the myristoyl group would have to move to prevent a steric clash with λ3 (Figure 2D) in a GTP-bound structure similar to hARF1Δ17·GTP. Myristoyl insertion in lipids could allow a GTP-like structure, and promote nucleotide exchange, by eliminating this potential clash. Thus, N-myristoylation would play an important regulatory role during guanine nucleotide exchange by ensuring that efficient exchange occurs only on the membrane surface.

The Myristoyl Group Contributes to yARF1·GTP-Membrane Interaction

Although GTP-loaded forms of yARF1are not sufficiently soluble in the absence of lipids to conduct NMR experiments, it was possible to conduct experiments on both myr(+)- and myr(−)-yARF1·GTP in the presence of small bicelles. The results are presented in Figure 3D. In comparison to correlation times extracted for both GDP-bound forms in the absence of bicelles (Figures 3A and 3B), there is a substantial increase (80%–100%) in correlation times for the GTP-bound forms. Given partial contribution from changes in viscosity, this may not be as large as expected for a rigid integration with the bicelle structure, but it likely indicates a high degree of bicelle-protein interaction. This is consistent with previous data suggesting that ARF·GTP is capable of stable membrane association both in the presence and absence of a myristoyl chain (Franco et al., 1993).

There is actually a small difference in correlation times for the myr(+) and myr(−) forms, with the myr(+) form being more immobilized. This can be seen in the averaged τ_c values, but also in a residue by residue comparison. Although resonances for the GTP forms were not assigned, chemical shift changes between myr(+)- and myr(−)-yARF1·GTP are very small, allowing residue by residue comparisons of τ_c. A systematic increase in τ_c is seen for the myr(+) form here as well. A difference in τ_c would not be expected if association is complete (as expected from the lack of solubility in the absence of lipids) and the structural properties of the protein-bicelle complexes are similar. A possible explanation is that the motion of the two proteins at the bicelle surface is different. Membrane/membrane-associated proteins generally have ns-μs timescale rotational or wobbling motions on the membrane surface. When this motion is on a timescale that is shorter or similar to that of the global tumbling motion of the protein-bicelle complex, it has significant effects on the effective rotational correlation time. The increase in τ_c of myr(+)- over myr(−)-yARF1·GTP could be due to decreased local motions of ARF when association is enhanced by lipid-myristoyl interaction. A decrease in local motion could entropically favor further associations with other accessory proteins (e.g., adaptor proteins) at the membrane surface. This may suggest an additional role for ARF myristoylation.

In summary, the data presented support a model in which the myristoyl group plays an important role during guanine nucleotide exchange (Franco et al., 1993, 1996). Structural comparisons of myr(+)-yARF1·GDP with ARFΔ17·GTP (Goldberg, 1998) and ARFΔ17·GTP/Sec7 (Goldberg, 1998; Renault et al., 2003) provide a structural basis for a possible regulatory function of the myristoyl group. Basically, its presence inhibits movement of protein elements necessary for nucleotide exchange, unless a membrane is available to accommodate the myristoyl chain. Hence, exchange occurs only after association with a membrane

surface. Comparison of the tendencies of various yARF1 forms to associate with large and small bicelles also provides insight into the role of myristoylation. Both ARF·GTP forms associate strongly with even small bicelles. However, the myristoyl group appears to further stabilize the interaction, which may be important for the interaction of ARF·GTP with other proteins on the membrane surface. In comparison, neither myr(−)-yARF1·GDP nor myr(+)-yARF1·GDP could be demonstrated to associate with small bicelles. However, using a larger bicelle, with a more extended bilayer surface, myr(+)-yARF1·GDP was found to have a substantial tendency to associate with a membrane surface, and to do so more strongly than myr(−)-yARF1·GDP. Although the inability to demonstrate this with small bicelles could simply be a reflection of weak binding, it is worth noting that an increased specificity for planar membranes would be consistent with the role of ARF as the initiator of membrane traffic carrier biogenesis.

EXPERIMENTAL PROCEDURES

Protein Expression and Purification

Full-length yARF1 was cloned into a pET20(b) (Novagen) vector using NdeI and XhoI sites. A thrombin cleavage site was introduced for removal of the C-terminal H_6 tag included in the vector. For production of myr(+)-yARF1, yARF1-pET20(b) was cotransformed with the pBB131 vector containing the human N-myristoyltransferase 1 (hNMT1) open reading frame into the BL-21(DE3) cell line. Cells were grown in M9 medium containing 1 g/l NH_4Cl, 2 g/l glucose, 100 mg/l ampicillin, and 50 mg/l kanamycin at 37°C until OD_{600nm} reached 0.5, at which point sodium myristate was added to 25 μM. IPTG (0.4 mM) was added when OD_{600nm} reached 1.0–1.1 and cells were grown at 28°C overnight. For production of perdeuterated ARF, freshly transformed cells were inoculated into 40 ml LB medium in H_2O. When OD_{600nm} reached 0.5–0.6, cells were spun down and resuspended in 200 ml M9 medium in H_2O. Growth continued until OD_{600nm} reached 0.5–0.6, at which point cells were spun down and resuspended in 1 liter M9 medium in D_2O with 2 g/l $^2D_7$-$^{13}C_6$-glucose and 1 g/l $^{15}NH_4Cl$. Sodium myristate was added to 25 μM at an OD_{600nm} of ~0.8 and IPTG was added to 0.4 mM at an OD_{600nm} of 1.0–1.2. After induction, cells were held at 37°C for 6 hr or at 28°C overnight.

Production of methyl-protonated protein in a partially perdeuterated background followed the aforementioned procedure except that 3,3-$^2D_2$-1,2,3,4-$^{13}C_4$-2-keto-butyrate (100 mg/l) and 3-$^2D_1$-1,2,3,4-$^{13}C_4$-2-keto-isovalerate (100 mg/l) were added together with sodium myristate (25 μM) ~1 hr before induction (OD_{600nm} = ~0.8). In addition, protonated $^{13}C_6$-glucose (2 g/l) was used here as the background carbon source. This allows a sufficient level of protonation on the methyl groups of Ala and Met for additional NOE measurements while preserving the spectral simplicity and favorable relaxation behavior of perdeuterated samples. The myristoylation efficiency was usually ~50%, with the other half dominated by lauroylated forms as suggested by electrospray ionization mass spectrometry and fatty acid analysis (data not shown). No steps were taken to isolate the myristoylated from the other acylated forms. Signals from the myristoylated ARF were selectively investigated through an isotope labeling strategy in which the myristoyl and the other fatty acids were differentially labeled.

For production of myr(−)-yARF1, yARF1-pET20(b) but not hNMT1-pBB131 was transformed, kanamycin was not included in the growth medium, and sodium myristate was not added; other growth conditions remain identical. Purification of myr(+)- and myr(−)-yARF1·GDP followed the same protocol. Proteins were first purified by affinity chromatography on a HisTrap column and the H_6 tag was removed with thrombin. Proteins were further subjected to ion-exchange chromatography on a Q-Sepharose column. A final yield of 20–30 mg of protein per liter of culture was usually achieved.

Preparation of Lipid-Containing Samples

For τ_c measurements, a 10% (w/v) small-bicelle solution containing DMPC and DHPC at a 1:4 molar ratio was employed. For interactions with bicelles of varying sizes, the total lipid concentration was fixed at 8%, with the relative amount of DMPC and DHPC adjusted as specified in the main text. Protein was maintained at a concentration of 0.5 mM in NMR buffer (10 mM K_2HPO_4-KH_2PO_4 [pH 7.0], 50 mM NaCl, 10 mM K_2SO_4, 2 mM $MgCl_2$, and 5 mM dithiothreitol) throughout these assays.

Guanine Nucleotide Exchange in Lipid-Containing Solution

myr(+)- or (−)-yARF1·GDP was first mixed with DMPC and DHPC to a final lipid concentration of 10% and a protein concentration of 0.5 mM in NMR buffer. GTP and EDTA were then added to 10 and 2 mM, respectively. The sample was incubated at room temperature overnight and $MgCl_2$ (to 2 mM) was added before transferring the sample to an NMR tube. The exchange resulted in a preparation containing mostly the GTP form (>3:2), as determined by the appearance of new chemical shift distinct HSQC crosspeaks, allowing relaxation time measurements specifically for this form.

NMR Spectroscopy

Spectra were acquired on 600, 800, and 900 MHz spectrometers (Varian) on samples containing 0.5–0.8 mM protein in NMR buffer. All experiments were conducted at 25°C. Backbone resonances were assigned using data from HNCACB, HN(CO)CA, HN(COCA)CB, and CBCA(CO)NH experiments on a fully protonated sample. Methyl groups in selectively protonated samples were assigned using a doubly enhanced, ^{13}C-excited CC_mH_m-TOCSY experiment modified from previously published pulse sequences (Permi et al., 2004; Yang et al., 2004). NOESY-^{15}N-HSQC on the same sample proved helpful in solving assignment ambiguities by correlating the methyl protons to the amides. A number of H_α and H_β protons were assigned based on HNHA, ^{1}H-^{1}H-TOCSY-^{15}N-HSQC, and NOESY-^{15}N-HSQC experiments collected on a fully protonated ^{15}N sample. The myristoyl protons were assigned using two-dimensional water-gated NOESY on a myristoyl-protonated, but otherwise highly perdeuterated, sample.

An attempt was made to selectively retrieve data on the myristoylated form of ARF in the presence of other acylated ARF species (mostly lauroylated) through the following approach. In preparations of fully perdeuterated protein, $^1H_{27}$-$^{12}C_{14}$-sodium myristate was supplemented in a growth medium containing D_2O and $^2D_7$-glucose, and thus the endogenous lauroyl group was expected to be perdeuterated whereas the majority of the myristoyl would come from the supplemented material and be protonated. A NOESY-^{15}N-HSQC experiment revealed crosspeaks to amide protons from the myristate but not from the other acyl groups. In the preparation of methyl-protonated, background-deuterated protein, $^1H_{27}$-$^{12}C_{14}$-sodium myristate was applied to a medium containing D_2O and protonated $^{13}C_6$-glucose. The endogenous lauroyl was thus expected to be ^{13}C labeled whereas most of the myristoyl adduct would be protonated and ^{12}C labeled. Thus, signals from the acyl groups can be eliminated by ^{13}C-filtered experiments. NOEs between myristoyl protons and methyl protons were revealed and assigned using ^{13}C-filtered-NOESY-^{13}C-edited-HSQC experiments. Sample panels from this experiment showing connections from myristoyl methyl and methylene groups to side chains of specific residues in the protein are given in Supplemental Data. The approach presumes minimal metabolic conversion of $^1H_{27}$-$^{12}C_{14}$-sodium myristate to a $^1H_{27}$-$^{12}C_{14}$-laurate species. We were unable to quantify this possible conversion and thus must acknowledge possible contamination of myristoyl with lauroyl data.

A negatively charged (50% 2-acrylamido-2-methyl-1-propanesulfonic acid + 50% acrylamide) compressed gel (Cierpicki and Bushweller, 2004) and a neutral (100% acrylamide) stretched gel (Sass et al., 2000) were employed to obtain two highly uncorrelated alignments for the measurement of residual dipolar couplings. These were measured from an interleaved TROSY-HSQC pair of acquisitions (Ottiger and Bax, 1998). The correlation coefficient between the two alignments is 0.02. Spin relaxation data for the extraction of correlation times were acquired with an experiment designed to directly detect chemical shift anisotropy–dipole-dipole crosscorrelated relaxation times (Liu and Prestegard, 2008).

Structural Determination

Structural calculation was conducted using a simulated annealing protocol provided in the CNS software (Brünger et al., 1998). Distance restraints were classified into three categories: strong (1.8–2.7 Å), medium (1.8–3.7 Å), and

weak (1.8–5.5 Å), based on the volumes of NOESY crosspeaks. Backbone dihedral angles were derived from N, HN, C_α, C_β, and C′ chemical shifts using the TALOS program (Cornilescu et al., 1999). Errors for NH RDCs were estimated from duplicate experiments. The force constants during simulated annealing were adjusted so that the final deviations between experimental and back-calculated RDCs were comparable to experimental errors (see Table 1). Force constants for D_{NH}, $D_{NC'}$, and $D_{HNC'}$ were ramped from 0.01 to 0.6, 0.3, and 0.3 kcal.mol^{-1}.Hz^{-2}, respectively.

ACCESSION NUMBERS

The resulting 15 lowest-energy structures have been deposited in the Protein Data Bank under ID code 2k5u. NMR assignments and constraint data have been deposited in the BioMagResBank under ID code 15809.

SUPPLEMENTAL DATA

Supplemental Data include two figures and can be found with this article online at http://www.cell.com/structure/supplemental/S0969-2126(08)00432-2.

ACKNOWLEDGMENTS

This work was supported by a grant from the National Institutes of Health (GM61268).

Received: September 22, 2008
Revised: October 25, 2008
Accepted: October 29, 2008
Published: January 13, 2009

REFERENCES

Amor, J.C., Harrison, D.H., Kahn, R.A., and Ringe, D. (1994). Structure of the human ADP-ribosylation factor 1 complexed with GDP. Nature *372*, 704–708.

Amor, J.C., Horton, J.R., Zhu, X., Wang, Y., Sullards, C., Ringe, D., Cheng, X., and Kahn, R.A. (2001). Structures of yeast ARF2 and ARL1: distinct roles for the N terminus in the structure and function of ARF family GTPases. J. Biol. Chem. *276*, 42477–42484.

Bigay, J., Gounon, P., Robineau, S., and Antonny, B. (2003). Lipid packing sensed by ArfGAP1 couples COPI coat disassembly to membrane bilayer curvature. Nature *426*, 563–566.

Bigay, J., Casella, J., Drin, G., Mesmin, B., and Antonny, B. (2005). ArfGAP1 responds to membrane curvature through the folding of a lipid packing sensor motif. EMBO J. *24*, 2244–2253.

Bonifacino, J.S. (2004). The GGA proteins: adaptors on the move. Nat. Rev. Mol. Cell Biol. *5*, 23–32.

Brown, H.A., Gutowski, S., Moomaw, C.R., Slaughter, C., and Sternweis, P.C. (1993). ADP-ribosylation factor, a small GTP-dependent regulatory protein, stimulates phospholipase D activity. Cell *75*, 1137–1144.

Brünger, A.T., Adams, P.D., Clore, G.M., Delano, W.L., Gros, P., Crosse-Kunstleve, R.W., Jiang, J.S., Kuszewski, J., Nilges, M., Pannu, N.S., et al. (1998). Crystallography & NMR system: a new software suite for macromolecular structure determination. Acta Crystallogr. D Biol. Crystallogr. *54*, 905–921.

Chardin, P., Paris, S., Antonny, B., Robineau, S., Béraud-Dufour, S., Jackson, C.L., and Chabre, M. (1996). A human exchange factor for ARF contains Sec7- and pleckstrin-homology domains. Nature *384*, 481–484.

Cierpicki, T., and Bushweller, J.H. (2004). Charged gels as orienting media for measurement of residual dipolar couplings in soluble and integral membrane proteins. J. Am. Chem. Soc. *126*, 16259–16266.

Cornilescu, G., Delaglio, F., and Bax, A. (1999). Protein backbone angle restraints from searching a database for chemical shift and sequence homology. J. Biomol. NMR *13*, 289–302.

Cukierman, E., Huber, I., Rotman, M., and Cassel, D. (1995). The ARF1 GTPase-activating protein: zinc-finger motif and Golgi-complex localization. Science *270*, 1999–2002.

Donaldson, J.G., Honda, A., and Weigert, R. (2005). Multiple activities for Arf1 at the Golgi complex. Biochim. Biophys. Acta *1744*, 364–373.

Franco, M., Chardin, P., Chabre, M., and Paris, S. (1993). Myristoylation is not required for GTP-dependent binding of ADP-ribosylation factor ARF1 to phospholipids. J. Biol. Chem. *268*, 24531–24534.

Franco, M., Chardin, P., Chabre, M., and Paris, S. (1996). Myristoylation-facilitated binding of the G protein $ARF1_{GDP}$ to membrane phospholipids is required for its activation by a soluble nucleotide exchange factor. J. Biol. Chem. *271*, 1573–1578.

Gillingham, A.K., and Munro, S. (2007). The small G proteins of the Arf family and their regulators. Annu. Rev. Cell Dev. Biol. *23*, 579–611.

Gizachew, D., and Oswald, R. (2006). NMR structural studies of the myristoylated N-terminus of ADP ribosylation factor 6 (Arf6). FEBS Lett. *580*, 4296–4301.

Glover, K.J., Whiles, J.A., Wu, G., Yu, N., Deems, R., Struppe, J.O., Stark, R.E., Komives, E.A., and Vold, R.R. (2001). Structural evaluation of phospholipid bicelles for solution-state studies of membrane-associated biomolecules. Biophys. J. *81*, 2163–2171.

Godi, A., Pertile, P., Meyers, R., Marra, P., Di Tullio, G., Iurisci, C., Luini, A., Corda, D., and De Matteis, M.A. (1999). ARF mediates recruitment of PtdIns-4-OH kinase-β and stimulates synthesis of PtdIns(4,5)P2 on the Golgi complex. Nat. Cell Biol. *1*, 280–287.

Godi, A., Di Campli, A., Konstantakopoulos, A., Di Tullio, G., Alessi, D.R., Kular, G.S., Daniele, T., Marra, P., Lucocq, J.M., and De Matteis, M.A. (2004). FAPPs control Golgi-to-cell-surface membrane traffic by binding to ARF and PtdIns(4)P. Nat. Cell Biol. *6*, 393–404.

Goldberg, J. (1998). Structural basis for activation of ARF GTPase: mechanisms of guanine nucleotide exchange and GTP-myristoyl switching. Cell *95*, 237–248.

Helms, J.B., Palmer, D.J., and Rothman, J.E. (1993). Two distinct populations of ARF bound to Golgi membranes. J. Cell Biol. *121*, 751–760.

Hill, K., Li, Y.W., Bennett, M., McKay, M., Zhu, X.J., Shern, J., Torre, E., Lah, J.J., Levey, A.I., and Kahn, R.A. (2003). Munc18 interacting proteins: ADP-ribosylation factor-dependent coat proteins that regulate the traffic of β-Alzheimer's precursor protein. J. Biol. Chem. *278*, 36032–36040.

Inoue, H., and Randazzo, P.A. (2007). Arf GAPs and their interacting proteins. Traffic *8*, 1465–1475.

Kahn, R.A., Kern, F.G., Clark, J., Gelmann, E.P., and Rulka, C. (1991). Human ADP-ribosylation factors. A functionally conserved family of GTP-binding proteins. J. Biol. Chem. *266*, 2606–2614.

Kahn, R.A., Randazzo, P., Serafini, T., Weiss, O., Rulka, C., Clark, J., Amherdt, M., Roller, P., Orci, L., and Rothman, J.E. (1992). The amino terminus of ADP-ribosylation factor (ARF) is a critical determinant of ARF activities and is a potent and specific inhibitor of protein transport. J. Biol. Chem. *267*, 13039–13046.

Kishore, N.S., Wood, D.C., Mehta, P.P., Wade, A.C., Lu, T., Gokel, G.W., and Gordon, J.I. (1993). Comparison of the acyl chain specificities of human myristoyl-CoA synthetase and human myristoyl-CoA:protein N-myristoyltransferase. J. Biol. Chem. *268*, 4889–4902.

Lavalette, D., Hink, M.A., Tourbez, M., Tétreau, C., and Visser, A.J. (2006). Proteins as micro viscosimeters: Brownian motion revisited. Eur. Biophys. J. *35*, 517–522.

Liu, Y., and Prestegard, J.H. (2008). Direct measurement of dipole-dipole/CSA cross-correlated relaxation by a constant-time experiment. J. Magn. Reson. *193*, 23–31.

Logsdon, J.M., and Kahn, R.A. (2004). The ARF family tree. In The ARF Family GTPases, R.A. Kahn, ed. (Dordrecht: Kluwer Academic Publishers), pp. 1–22.

Losonczi, J.A., and Prestegard, J.H. (1998). Nuclear magnetic resonance characterization of the myristoylated, N-terminal fragment of ADP-ribosylation factor 1 in a magnetically oriented membrane array. Biochemistry *37*, 706–716.

Luchette, P.A., Vetman, T.N., Procsser, R.S., Hancock, R.E., Nieh, M.P., Glinkda, C.J., Krueger, S., and Katsaras, J. (2001). Morphology of fast-tumbling bicelles: a small angle neutron scattering and NMR study. Biochim. Biophys. Acta *1513*, 83–94.

Nie, Z., Hirsch, D.S., and Randazzo, P.A. (2003). Arf and its many interactors. Curr. Opin. Cell Biol. *15*, 396–404.

Ottiger, M., and Bax, A. (1998). Determination of relative N-H^N, N-C′, C^α-C′, and C^α-H^α effective bond lengths in a protein by NMR in a dilute liquid crystalline phase. J. Am. Chem. Soc. *120*, 12334–12341.

Permi, P., Tossavainen, H., and Hellman, M. (2004). Efficient assignment of methyl resonances: enhanced sensitivity by gradient selection in a DE-MQ-(H)CC^mHt^m-TOCSY experiment. J. Biomol. NMR *30*, 275–282.

Pervushin, K., Riek, R., Wider, G., and Wüthrich, K. (1997). Attenuated T_2 relaxation by mutual cancellation of dipole-dipole coupling and chemical shift anisotropy indicates an avenue to NMR structures of very large biological macromolecules in solution. Proc. Natl. Acad. Sci. USA *94*, 12366–12371.

Peyroche, A., Paris, S., and Jackson, C.L. (1996). Nucleotide exchange on ARF mediated by yeast Gea1 protein. Nature *384*, 479–481.

Randazzo, P.A., and Kahn, R.A. (1995). Myristoylation and ADP-ribosylation factor function. Methods Enzymol. *257*, 128–135.

Randazzo, P.A., Terui, T., Sturch, S., Fales, H.M., Ferrige, A.G., and Kahn, R.A. (1995). The myristoylated amino-terminus of ADP-ribosylation factor-1 is a phospholipid-sensitive and GTP-sensitive switch. J. Biol. Chem. *270*, 14809–14815.

Renault, L., Guibert, B., and Cherfils, J. (2003). Structural snapshots of the mechanism and inhibition of a guanine nucleotide exchange factor. Nature *426*, 525–530.

Rosen, M.K., Gardner, K.H., Willis, R.C., Parris, W.E., Pawson, T., and Kay, L.E. (1996). Selective methyl group protonation of perdeuterated proteins. J. Mol. Biol. *263*, 627–636.

Ross, P.D., and Minton, A.P. (1977). Hard quasispherical model for the viscosity of hemoglobin solutions. Biochem. Biophys. Res. Commun. *76*, 971–976.

Sass, H.J., Musco, G., Stahl, S.J., Wingfield, P.T., and Grzesiek, S. (2000). Solution NMR of proteins within polyacrylamide gels: diffusional properties and residual alignment by mechanical stress or embedding of oriented purple membranes. J. Biomol. NMR *18*, 303–309.

Seidel, R.D., III, Amor, J.C., Kahn, R.A., and Prestegard, J.H. (2004). Conformational changes in human Arf1 on nucleotide exchange and deletion of membrane-binding elements. J. Biol. Chem. *279*, 48307–48318.

Serafini, T., Orci, L., Amherdt, M., Brunner, M., Kahn, R.A., and Rothman, J.E. (1991). ADP-ribosylation factor is a subunit of the coat of Golgi-derived COP-coated vesicles: a novel role for a GTP-binding protein. Cell *67*, 239–253.

Styers, M., and Faundez, V. (2004). Heterotetrameric coat protein-ARF interactions. In ARF Family GTPases, R.A. Kahn, ed. (Dordrecht: Kluwer Academic Publishers), pp. 259–281.

Tanaka, T., Ames, J.B., Harvey, T.S., Stryer, L., and Ikura, M. (1995). Sequestration of the membrane-targeting myristoyl group of recoverin in the calcium-free state. Nature *376*, 444–447.

Tang, C., Loeliger, E., Luncsford, P., Kinde, I., Beckett, D., and Summers, M.F. (2004). Entropic switch regulates myristate exposure in the HIV-1 matrix protein. Proc. Natl. Acad. Sci. USA *101*, 517–522.

Tanigawa, G., Orci, L., Amherdt, M., Ravazzola, M., Helms, J.B., and Rothman, J.E. (1993). Hydrolysis of bound GTP by ARF protein triggers uncoating of Golgi-derived COP-coated vesicles. J. Cell Biol. *123*, 1365–1371.

Tjandra, N., and Bax, A. (1997). Direct measurement of distances and angles in biomolecules by NMR in a dilute liquid crystalline medium. Science *278*, 1111–1114.

Tolman, J.R., Flanagan, J.M., Kennedy, M.A., and Prestegard, J.H. (1995). Nuclear magnetic dipole interactions in field-oriented proteins: information for structure determination in solution. Proc. Natl. Acad. Sci. USA *92*, 9279–9283.

Vold, R.R., and Prosser, R.S. (1996). Magnetically oriented phospholipid bilayered micelles for structural studies of polypeptides. Does the ideal bicelle exist? J. Magn. Reson. B *113*, 267–271.

Weiss, O., Holden, J., Rulka, C., and Kahn, R.A. (1989). Nucleotide binding and cofactor activities of purified bovine brain and bacterially expressed ADP-ribosylation factor. J. Biol. Chem. *264*, 21066–21072.

Yang, D., Zheng, Y., Liu, D., and Wyss, D.F. (2004). Sequence-specific assignments of methyl groups in high-molecular weight proteins. J. Am. Chem. Soc. *126*, 3710–3711.

Zozulya, S., and Stryer, L. (1992). Calcium-myristoyl protein switch. Proc. Natl. Acad. Sci. USA *89*, 11569–11573.